Journal of Alzheimer's Disease 88 (2022) 1137–1145
DOI 10.3233/JAD-220314
IOS Press

Noninvasive Antemortem Detection of Retinal Prions by a Fluorescent Tracer

Patricia Aguilar-Calvo[a,*], Alejandro M. Sevillano[a,1], Suhail Rasool[b,2], Kevin J. Cao[c,3], Lyndsay M. Randolph[b], Robert A. Rissman[d], Stella T. Sarraf[b], Jerry Yang[c] and Christina J. Sigurdson[a,e,f,*]
[a]*Department of Pathology, UC San Diego, La Jolla, CA, USA*
[b]*Amydis, Inc., San Diego, CA*
[c]*Department of Chemistry and Biochemistry, University of California, San Diego, La Jolla, CA, USA*
[d]*Department of Neurosciences, UC San Diego, La Jolla, CA, USA*
[e]*Department of Pathology, Microbiology, and Immunology, UC Davis, Davis, CA, USA*
[f]*Department of Medicine, UC San Diego, La Jolla, CA, USA*

Handling Associate Editor: Inga Zerr

Accepted 19 May 2022
Pre-press 20 June 2022

Abstract.
Background: Neurodegenerative diseases are widespread yet challenging to diagnose and stage antemortem. As an extension of the central nervous system, the eye harbors retina ganglion cells vulnerable to degeneration, and visual symptoms are often an early manifestation of neurodegenerative disease.
Objective: Here we test whether prion protein aggregates could be detected in the eyes of live mice using an amyloid-binding fluorescent probe and high-resolution retinal microscopy.
Methods: We performed retinal imaging on an experimental mouse model of prion-associated cerebral amyloid angiopathy in a longitudinal study. An amyloid-binding fluorophore was intravenously administered, and retinal imaging was performed at timepoints corresponding to early, mid-, and terminal prion disease. Retinal amyloid deposits were quantified and compared to the amyloid load in the brain.
Results: We report that by early prion disease (50% timepoint), discrete fluorescent foci appeared adjacent to the optic disc. By later timepoints, the fluorescent foci surrounded the optic disc and tracked along retinal vasculature.
Conclusion: The progression of perivascular amyloid can be directly monitored in the eye by live imaging, illustrating the utility of this technology for diagnosing and monitoring the progression of cerebral amyloid angiopathy.

Keywords: Alzheimer's disease, amyloid, cerebral amyloid angiopathy, diagnostic, early diagnosis, eye, fluorophore, neurodegeneration, prion, protein misfolding, retina, retinal amyloid

[1]Current address: Department of Clinical Cancer Prevention, The University of Texas MD Anderson Cancer Center, Houston, TX, USA.
[2]Current address: Truebinding Inc., Foster City, CA, USA.
[3]Current address: Department of Molecular and Cell Biology, University of California, Berkeley, Berkeley, CA, USA.

*Correspondence to: Drs. Patricia Aguilar-Calvo and Christina J. Sigurdson, Department of Pathology, UC San Diego, 9500 Gilman Dr., La Jolla, CA 92093-0612, USA. Tel.: +1 858 534 0978; E-mail: p2aguilar@health.ucsd.edu (P. Aguilar-Calvo) and csigurdson@health.ucsd.edu (C.J. Sigurdson).

INTRODUCTION

Neurodegenerative disorders, including Alzheimer's disease (AD), cerebral amyloid angiopathy (CAA), Parkinson's disease, and prion disease, affect more than 55 million people worldwide [1]. Protein aggregates are a central feature, accumulating in the brain and contributing to synaptic loss and neuronal death. Non-invasive, inexpensive screening technologies are urgently needed for early diagnosis and monitoring disease progression. Patients with neurodegenerative disease often present with visual impairment as an early symptom [2, 3]; for example, patients with prion disease frequently develop diplopia, supranuclear palsies, and loss of vision in early disease stages [4–6] and thus may visit an ophthalmologist [7]. Given that the eye is an extension of the central nervous system (CNS), and that amyloid-β (Aβ), α-synuclein, and prion aggregates may develop in the human retina [8–12], antemortem detection of retinal aggregates using imaging could offer a practical approach to diagnose early disease as well as track aggregate load and response to therapy.

Efforts to use fluorescence imaging to detect retinal amyloid in mouse models and humans with neurodegenerative disease have yielded inconsistent results, potentially due to structural differences in the amyloid-binding probes employed. Congophilic dyes bind to amyloid with high specificity and have been used for decades to detect amyloid in postmortem tissue [13–15]. More recently, the natural fluorophore curcumin was reported to bind retinal Aβ antemortem in an AD mouse model and in patients [16–18]. However, the bioavailability of curcumin is low, and high oral doses (1 g curcumin per day) over 2 to 10 days were required to visualize the purported Aβ deposits in AD patients [16, 18]. Additional fluorescent dyes with high signal-to-noise ratios have been used to visualize amyloid deposits in tissue and to distinguish between amyloids of differing protein composition or conformation [19–22]. For example, the ARCAM-1 fluorophore selectively labels Aβ-containing deposits in mouse and human retina [19], but the poor solubility of this fluorophore precludes its further development for use in human patients.

A significant challenge for development of new probes with suitable properties for the antemortem detection of retinal amyloid is the lack of reliable experimental model systems with abundant ocular amyloid deposits [19]. To determine whether retinal amyloid could be detected antemortem using retinal imaging microscopy, here we evaluate a more soluble analog of ARCAM-1, known as ARCAM-11, in an experimental mouse model with ocular prion deposits. We investigated prion-infected tg(GPI-PrP) mice (line tg44), which express glycosylphosphatidylinositol (GPI)-anchorless PrP^C that is secreted into the extracellular space [20]. Prion-infected tg(GPI-PrP) mice develop multifocal, perivascular prion plaques in the brain, similar to those observed in humans with CAA due to Aβ, as well as deposits within the optic nerve and retina (ganglion and inner nuclear layers) [21]. The GPI-anchorless prion aggregates accumulate adjacent to the capillary and arteriolar basement membranes and eventually replace the vessel wall with amyloid [22, 23]. Therefore, prion-infected tg(GPI-PrP) mice are a useful model of cerebrovascular amyloid disease. In a longitudinal study, we initially observed amyloid retinal deposits adjacent to the optic disc, and by later timepoints, extensive amyloid had also deposited radially along blood vessels. Collectively, these data show that as amyloid load rises in the brain, an increase in retinal vascular aggregates could be visualized in live mice using an amyloid binding dye, indicating the utility of retinal imaging for the early diagnosis and monitoring of prion-induced, and potentially also Aβ-induced, CAA.

MATERIALS AND METHODS

Synthesis of fluorescent probes

The synthesis and characterization of ARCAM-1 was previously reported by Cao et al. [24]. ARCAM-11 was modeled after ARCAM-1, considering modifications to the structure that enhanced aqueous solubility (Supplementary Table 1) and improved other pharmacological properties. ARCAM-11 was provided by Amydis for this study and had a purity of 98%.

Study approval

All animal studies were approved by the Institutional Animal Care and Use Committee at UC San Diego. Protocols were performed in strict accordance with good animal practices, as described in the Guide for the Use and Care of Laboratory Animals published by the National Institutes of Health.

Prion infections and retinal imaging

Male and female tg(GPI-PrP) mice [20] ($n = 29$, 6–8 weeks old) were anesthetized with ketamine and xylazine and inoculated into the left parietal cortex with 30 μl of 1% mock brain homogenate or prion-infected brain homogenate prepared from terminally ill tg(GPI-PrP) mice infected with prions (strain GPI-ME7), or served as uninculated controls. Mice were monitored three times per week for the development of terminal prion disease including ataxia, kyphosis, stiff tail, hind leg clasp, and hind leg paresis.

For the fluorescence retinal imaging experiments, prion-inoculated (4–6 mice per timepoint) and mock- or uninoculated mice (3–5 mice per timepoint) were anesthetized with ketamine and xylazine prior to retinal examination with a Phoenix Micron IV retinal microscope for fluorescence retinal imaging (Phoenix Research Laboratories, Pleasanton, CA). An initial retinal scan was performed using the bright field and fluorescent light source (450 nm excitation) and images were collected. Freshly prepared ARCAM-1 (100 μL of 10 mg/mL in 20% DMSO/80% propylene glycol) or ARCAM-11 (100 μL of 2 mg/mL in phosphate-buffered saline) was intraperitoneally or intravenously administered, respectively, and retinal images were collected for 20–30 min. Animals were then euthanized and the imaged eye (right) was either formalin-fixed for flat-mount [method previously published in [19]], or frozen for biochemical studies. The left eye was embedded in optimal cutting temperature (OCT) compound and frozen on dry ice for cryosections. The left and right hemibrains were immediately fixed in formalin or frozen for histological or biochemical studies, respectively. A schematic of the experimental design is displayed in Fig. 2A (created with BioRender™).

Immunohistochemical stains

The formalin-fixed brain was treated for 1 h in 96% formic acid, post-fixed in formalin, cut into 2 mm transverse sections, and paraffin-embedded for histological analysis. Five-micron sections were cut onto positively charged glass slides and immunostained using an anti-PrP antibody [SAF84: epitope in the globular domain, amino acids 160–170 of mouse PrP (Cayman Chemical; 1:1,200)]. Immunostaining was performed on an automated tissue immunostainer (Ventana Discovery Ultra, Ventana Medical Systems, Inc) with cell conditioning 1 (CC1) and protease (P2) antigen retrieval, respectively.

For immunofluorescence, unfixed OCT-embedded brain sections were used. Ten-micron sections were cut into positively charged slides, dried at room temperature for 1 h, hydrated by passage of sections through an ethanol gradient (100%, 90%, 70%) and fixed with 4% paraformaldehyde for 30 min. Sections were next washed in water for 5 min, treated with 5μg/ml of proteinase-K (PK) for 10 min to digest PrP^C, and washed in water for 7 min. Slides were then placed in citrate buffer (pH 6), heated in a pressure cooker for 20 min, cooled for 5 min, and washed in distilled water. Sections were immunostained with anti-PrP antibody (SAF84) for 1 h, followed by anti-mouse biotin (Jackson Immunolabs) for 30 min, and then streptavidin–HRP (Jackson Immunoresearch) for 45 min. The nuclei were stained with 4′,6-diamidino-2-phenylindole (DAPI).

Tissue staining with amyloid-binding fluorophores

Unfixed OCT-embedded eye and brain sections were stained with ARCAM-1 and ARCAM-11 as previously described [19]. Ten-micron sections were cut into positively charged slides, dried at room temperature for 1 h and then hydrated by passage of sections through an ethanol gradient (100%, 90%, 70%) followed by distilled water (5 min each). Slides were incubated in phosphate-buffered saline (PBS) for 30 min and incubated in 60 μM ARCAM-1 or ARCAM-11 in PBS for 30 min at room temperature. The slides were then rinsed three times with PBS, stained with DAPI, and coverslipped using Prolong Gold Antifade mounting media (ThermoFisher).

Western blot of brain and eye

Brain and eye tissues were homogenized in PBS using a Beadbeater™ tissue homogenizer. The total protein concentration was measured in 10% brain and eye homogenates by bicinchoninic acid assay (Pierce). For quantifying PK-resistant prion aggregates (PrP^{Sc}) in brain, 80 μg of total protein were incubated with 2% sarcosyl in PBS (final concentration) at 37°C for 30 min, digested with 50 μg/ml PK at 37°C for 30 min and the reaction stopped by boiling samples for 5 min in LDS loading buffer (Invitrogen). Samples were electrophoresed in 10% Bis-Tris gel (Invitrogen) and

transferred to a nitrocellulose membrane by wet blotting. Membranes were incubated with monoclonal antibody POM19 (discontinuous epitope at C-terminal domain, including amino acids 201–225 [25]) followed by incubation with an HRP-conjugated anti-mouse IgG secondary antibody (Jackson ImmunoResearch). The blots were developed using a chemiluminescent substrate (ECL detection kit, ThermoScientific) and visualized using a Fuji LAS 4000 imager.

PrP^{Sc} from 10% eye homogenates in PBS was concentrated by sodium phosphotungstic acid (NaPTA) precipitation prior to immunoblotting. Briefly, 500 μg of protein was incubated in 2% sarcosyl (final concentration) in PBS at 37°C for 30 min, digested with benzonase™ (Sigma-Aldrich) followed by treatment with 20 μg/ml PK at 37°C for 30 min. After addition of 4% NaPTA to a 170 mM $MgCl_2$ solution containing protease inhibitors (Complete TM, Roche), extracts were incubated at 37°C for 30 min and centrifuged at 18,000 × *g* for 30 min at 25°C. Pellets were resuspended in 2% sarcosyl prior to electrophoresis and immunoblotting.

Image J quantifications

For quantitative analysis of PrP^{Sc} deposition in retina, images obtained with the Phoenix Micron IV fluorescence rodent retinal imaging system were converted to grayscale (16 bits) with FIJI (an ImageJ-based image processing software) to distinguish between areas of fluorophore-labeling and background. The area covered by fluorescently-labeled prion deposits was determined using a standardized histogram-based threshold technique using a macro that we developed to demarcate the prion deposits by the pixel intensity, and then subjected to "Measure" analysis.

PrP^{Sc} deposition in immunostained brain sections was measured by scanning slides with a Zeiss AxioImager, converting images into TIFF files, and quantifying PrP^{Sc} with FIJI software as described for the retina.

RESULTS

ARCAM-1 selectively binds to prion aggregates

We first tested whether ARCAM-1 binds prion plaques *ex vivo* in brain sections of prion-infected tg(GPI-PrP) mice that develop vascular plaques (prion-associated CAA). We performed labeling of adjacent brain sections with either ARCAM-1 or an anti-prion antibody and observed that the ARCAM-1 bound specifically to plaque-like deposits in the prion-infected brain, with no labelling of the mock control brain sections (Fig. 1A). To next determine whether ARCAM-1 crosses the blood retinal barrier (BRB) and binds prion aggregates in live mice, we injected mice intraperitoneally with ARCAM-1. Retinal imaging was performed pre- and 1 min post-fluorophore injection in live uninfected and terminal prion-infected mice using the Phoenix Micron IV microscope (450 nm excitation). We observed bright fluorescent deposits surrounding the optic disc and along retinal vessels immediately post-injection (Fig. 1B). A postmortem retinal flat-mount of this same mouse revealed fluorescent aggregates around the optic disc and along the vasculature (Fig. 1C), similar to vascular aggregates observed in the brain of prion-infected tg(GPI-PrP) mice [20]. ARCAM-1 and PrP antibody immunolabelling of adjacent frozen sections confirmed that the retinal PrP^{Sc} was labelled by ARCAM-1 (Fig. 1D). Collectively, these results indicate that ARCAM-1 crosses the BRB and binds retinal perivascular amyloid in live prion-infected mice.

Retinal prion deposits detected near optic disc in early disease (50% timepoint)

The poor solubility of ARCAM-1 in aqueous solutions limits its use in humans. A newly developed fluorophore (ARCAM-11) was next tested for the detection of retinal amyloid in cohorts of live mice over time. This fluorophore had a similar fluorogenic core as ARCAM-1 but contains pharmacophore elements that render this molecule superior in aqueous solubility compared to ARCAM-1 [by four orders of magnitude (Supplementary Table 1)]. We intracerebrally inoculated tg(GPI-PrP) mice with GPI-anchorless prion-infected or mock control brain, and performed retinal imaging on cohorts of mice injected intravenously with ARCAM-11 at early, mid-, and terminal disease timepoints (50%, 75%, and 100%) (Fig. 2A). Retinal amyloid was again readily detected and was visible by 1 min post-injection (Fig. 2B).

At the 50% timepoint, prion-infected mice ($n = 6$) showed mild kyphosis. No retinal lesions were observed by brightfield or fluorescent microscopy prior to probe exposure (Fig. 2C). However, after intravenous administration of ARCAM-11, four of six prion-inoculated mice showed punctate fluores-

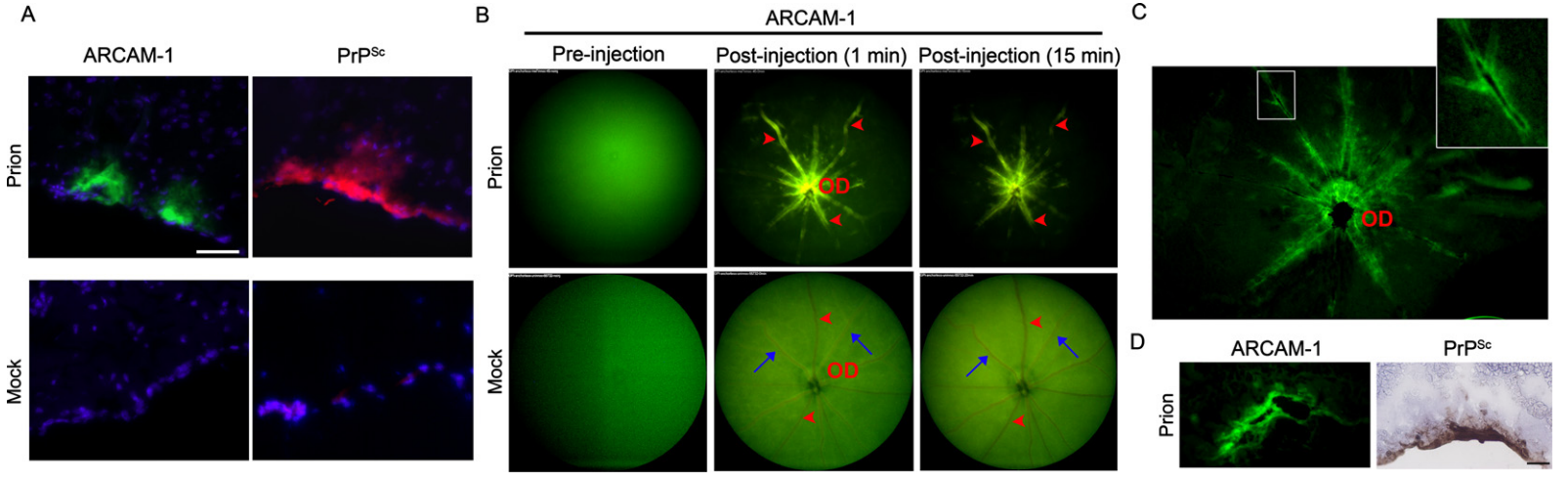

Fig. 1. ARCAM-1 labels prion aggregates in brain and retina. A) Brain sections (cortex) from prion-infected or mock-inoculated tg(GPI-PrP) mice stained with ARCAM-1 probe or immunolabelled for PrP^{Sc} show the probe binds submeningeal plaque-like deposits that appear similar to PrP^{Sc}. Scale bar = 50 μm. B) Real-time retinal imaging on mock or prion-exposed tg(GPI-PrP) mice, pre- and post-ARCAM-1 injection. Unbound ARCAM-1 appeared within the vasculature by one minute and rapidly disappeared (B, blue arrows); the remaining fluorescence corresponds to ARCAM-1 labeled amyloid. Fluorescent deposits surround the optic disc (OD) and retinal vessels extending from the disc (red arrowheads) in prion-infected mice (right eye for all mice). C) A retinal flat-mount from the same prion-infected tg(GPI-PrP) mouse shown in (B) confirms that fluorescently-labelled deposits surround the optic disc and retinal vessels. Inset shows fibrillar deposits surrounding a retinal vessel. D) Representative images of ARCAM-1- and PrP-immunolabelled cryosections show fluorescent ARCAM-1 in the retinal ganglion layer and a similar PrP^{Sc} localization in the -immunolabelled contralateral eye (same prion-inoculated tg(GPI-PrP) mouse from B and C). Scale bar = 200 μm.

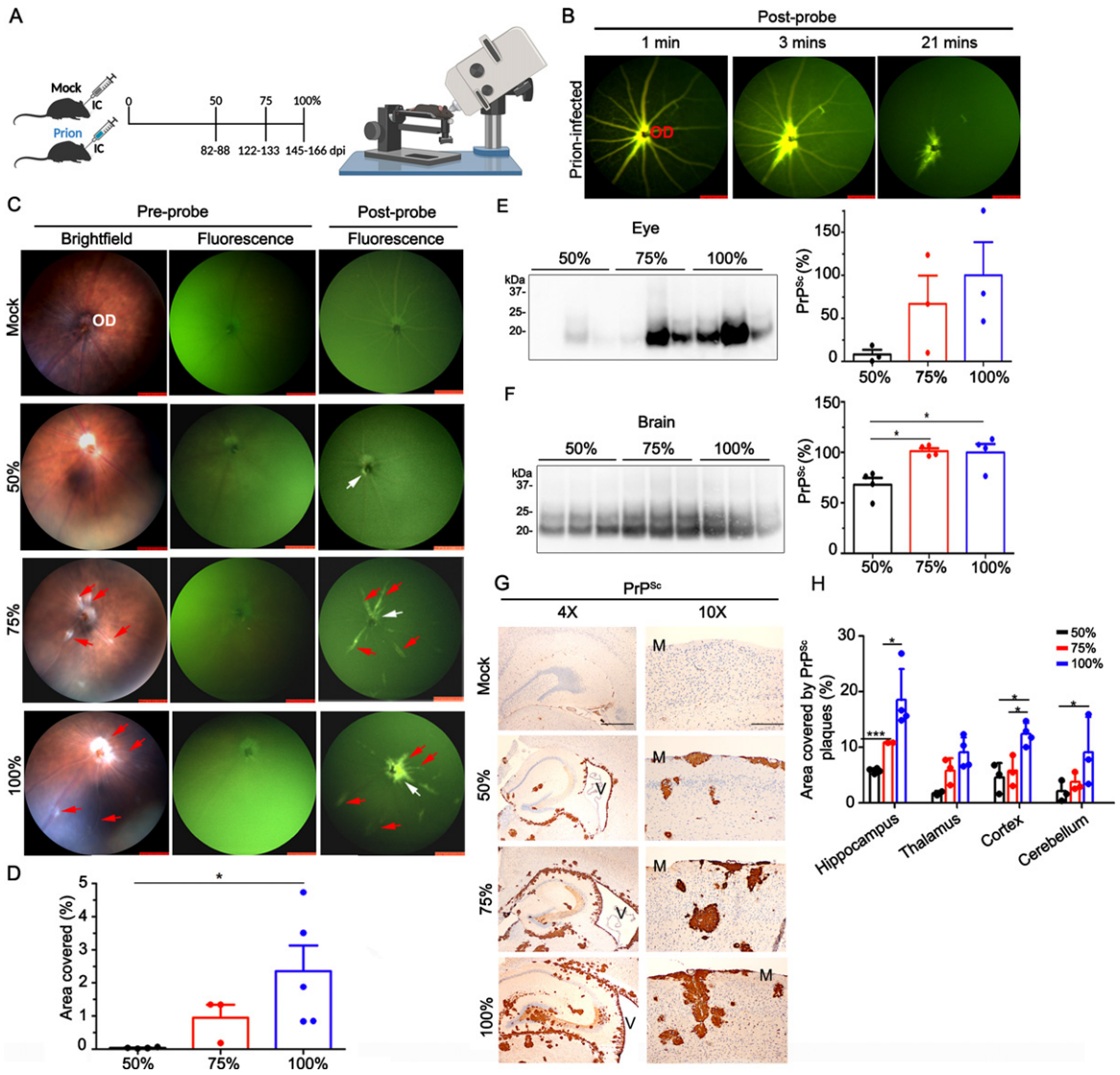

Fig. 2. ARCAM-11 fluorophore labels retinal prion aggregates at early disease. A) Schematic representation of the retinal imaging study (IC, intracerebral). B) Retinal images from prion-infected tg(GPI-PrP) mice, post-ARCAM-11 injection (elapsed post-injection time shown in minutes; OD, optic disc) (right eye for all mice). The ARCAM-11 fluorophore is detected in the vasculature and retina within the first minute post-injection. By 21 minutes, the probe is bound to retinal deposits and is no longer visible in the vasculature. C) ARCAM-11-labeled deposits occupy an increasingly larger area in the prion-infected tg(GPI-PrP) mice imaged at later disease timepoints (different animals at each timepoint, noted as 50%, 75%, and 100%). White arrows indicate fluorescently-labeled deposits on the optic disc, and red arrows indicate cotton-wool spots and show the co-localization with the fluorescently-labeled deposits. No mock-inoculated or uninoculated tg(GPI-PrP) mice showed white foci or fluorescent deposits at any timepoint. D) Graphs show that the retinal area having fluorescent deposits increases in mice imaged at later timepoints. E) Immunoblots and quantification of PrP^{Sc} levels in eye homogenates from prion-infected tg(GPI-PrP) mice at timepoints from 50% to 100% (normalized to the PrP^{Sc} average at terminal disease). F) Immunoblots of PrP^{Sc} in brain homogenates and corresponding quantification. G) Hippocampal (left) and cortical (right) sections immunolabeled for PrP reveal GPI-anchorless PrP^{Sc} accumulating perivascularly, periventricularly (V = ventricle), and adjacent to the meninges (M). Scale bar = 100 μm. H) The percent area covered by GPI-anchorless plaques in hippocampus, cerebral cortex, and cerebellum increased with time. $^{*}p < 0.05$, $^{***}p < 0.001$, One-way ANOVA with Tukey's post-test (D-F) and two-way ANOVA with Bonferroni post-test (H).

cent deposits adjacent to the optic disc (Fig. 2C, white arrow), which fluoresced approximately 1 min post-injection and continued to fluoresce throughout the imaging period (25–30 min). The fluorescent deposits comprised up to 0.2% of the retinal area imaged (Fig. 2D).

At the 75% timepoint, most prion-inoculated mice ($n = 4$) showed kyphosis and tip-toe walking. Strikingly, retinal brightfield imaging revealed white foci surrounding the optic disc of all mice, with two mice additionally showing perivascular white foci radiating centrifugally from the disc (Fig. 2C, red arrows), reminiscent of cotton wool spots in the retina of AD-affected patients [26, 27]. ARCAM-11 co-localized with the white foci from the first minute post-injection in three mice (one died during imaging) Fig. 2C, arrows), revealing deposits that were 7- to 10-fold larger than those observed at the 50% timepoint and affecting approximately 1.4% of the imaged retina (Fig. 2D).

The terminal prion-inoculated mice ($n = 6$) showed signs of ataxia, weight loss, and hind leg clasp. Retinal brightfield imaging revealed prominent white foci surrounding the optic disc and radially tracking dorsal and ventral retinal vessels (Fig. 2C). Following ARCAM-11 administration, all six mice showed fluorescent retinal deposits surrounding the optic disc and extending from the disc along the vessels (Fig. 2C, arrows), again co-localizing with the white foci. The retinal area containing fluorescent deposits was 2 to 4-fold larger than at the 75% timepoint and varied from 0.8% to 4.7% ($2.4 \pm 1.7\%$) of the imaged retina (Fig. 2D). No mock- or uninoculated tg(GPI-PrP) mice ($n = 13$) showed retinal abnormalities or fluorescent deposits at any timepoint (Fig. 2C).

To determine whether there was a correlation between brain and ocular PrP^{Sc} levels, we measured PrP^{Sc} levels in brain and globe lysates by immunoblotting using the anti-PrP antibody POM19 [25]. While brain PrP^{Sc} levels were similar among the mice within each timepoint, ocular PrP^{Sc} levels were more variable (Fig. 2E, F). Ocular PrP^{Sc} was detected at the 50% timepoint (Fig. 2E), yet the levels were low ($8 \pm 5\%$ of terminal level). By the 75% timepoint, ocular PrP^{Sc} levels were markedly higher ($67 \pm 33\%$ of the terminal level), suggesting prion spread into the eye in early to mid-disease (Fig. 2E). By comparison, PrP^{Sc} levels in the brain were high at the 50% timepoint ($68 \pm 7\%$ of terminal disease level) (Fig. 2F) and had increased by the 75% timepoint with little measureable change by terminal disease. Histologically, perivascular plaques at the 50% timepoint targeted predominantly the hippocampus and cerebral cortex, whereas at the 75% timepoint, plaques were larger and distributed more broadly across the brain, to include the thalamus and cerebellum (Fig. 2G, H). By the 100% timepoint, certain brain regions (i.e., cerebral cortex) showed a still higher PrP^{Sc} plaque area (Fig. 2G, H), an increase not detectable in the immunoblots of hemibrain lysates. Collectively, these data show that in the tg(GPI-PrP) mouse model of prion disease, extensive retinal vascular amyloid was identified antemortem by early disease using a fluorescent amyloid binding dye and retinal microscopy. These studies reveal a tractable ocular amyloid model for future development of topical amyloid binding dyes for clinical use.

DISCUSSION

Efficient diagnosis of neurodegenerative disease is critical to initiating early intervention, prior to extensive synapse loss. Here we show an experimental model system with abundant ocular amyloid, facilitating the evaluation of a peripherally administered fluorophore. The fluorophore rapidly and specifically bound to ocular amyloid with a high signal intensity, enabling early antemortem amyloid detection using standard retinal imaging cameras and providing a clear proof-of-concept.

The present study is the first report of white foci, or "cotton wool spots", in the retina of prion-affected mice, similar to those observed in AD patients [16, 26, 27]. The white, variably-sized foci were visible in the retina of all mice by the 75% timepoint at sites similar to the fluorescent probe, presumably bound to PrP^{Sc}. These ocular lesions, which can result from vascular insufficiency and neuronal loss, have been reported in patients with vascular dementia, and are associated with accelerated rates of cognitive decline [26–30]. Here the co-localization of prions with cotton wool spots in the prion-infected mice suggests that vascular amyloid should be also considered among the differentials for white foci in the retina.

Our studies provide evidence supporting the further development of amyloid-binding probes as an adjunct screening method for the antemortem diagnosis of neurodegenerative disease, particularly diseases characterized by extracellular amyloid, such as AD and GPI-anchorless prion disease [for example, caused by nonsense mutations in *PRNP* (Q145X, Q160X, or Q163X)] [31]. Patients with familial prion disease typically have no known family history of disease due to misdiagnosis, low penetrance, or *de novo* occurrence [32–34]. Retinal imaging offers a rapid, low cost tool for screening or monitoring CNS amyloid load [16, 35, 36] compared to electroencephalography, positron emission tomog-

raphy or magnetic resonance imaging. Moreover, fluorophores that emit at different maximal $\lambda_{emission}$ when bound to amyloids of different protein composition offer an additional advantage as an aid in differential disease diagnosis [37–39].

ACKNOWLEDGMENTS

We thank Drs. Michael Oldstone and Bruce Chesebro for providing the tg44 mice, Dr. Jen Ngolab and Michael Mante for technical support, Jin Wang and the animal care team at UC San Diego for excellent animal care, and Drs. Peter Vanderklish and Ali Tafreshi for critical review of the manuscript. This study was supported by the National Institutes of Health grants NS069566 (CJS), NS076896 (CJS), K99 AG061251 (PAC), RF1AG062362 (JY) and R43AG057421 (SS), as well as the Ramón Areces Foundation (PAC).

Authors' disclosures available online (https://www.j-alz.com/manuscript-disclosures/22-0314r1).

SUPPLEMENTARY MATERIAL

The supplementary material is available in the electronic version of this article: https://dx.doi.org/10.3233/JAD-220314.

REFERENCES

[1] World Health Organization BHU (2021) World Health Organization, https://cdn.who.int/media/docs/default-source/mental-health/dementia/who_dementia-infographic_2021-09-23_dv.pdf?sfvrsn=d9ecdc14_3.

[2] Sadun AA, Borchert M, DeVita E, Hinton DR, Bassi CJ (1987) Assessment of visual impairment in patients with Alzheimer's disease. *Am J Ophthalmol* **104**, 113-120.

[3] Katz B, Rimmer S (1989) Ophthalmologic manifestations of Alzheimer's disease. *Surv Ophthalmol* **34**, 31-43.

[4] Brown P, Gibbs CJ, Jr., Rodgers Johnson P, Asher DM, Sulima MP, Bacote A, Goldfarb LG, Gajdusek DC (1994) Human spongiform encephalopathy: The National Institutes of Health series of 300 cases of experimentally transmitted disease. *Ann Neurol* **35**, 513-529.

[5] Armstrong RA (2006) Creutzfeldt-Jakob disease and vision. *Clin Exp Optom* **89**, 3-9.

[6] Lueck CJ, McIlwaine GG, Zeidler M (2000) Creutzfeldt-Jakob disease and the eye. II. Ophthalmic and neuro-ophthalmic features. *Eye* **14**, 291-301.

[7] Hamaguchi T, Noguchi-Shinohara M, Nakamura Y, Sato T, Kitamoto T, Mizusawa H, Yamada M (2007) Ophthalmic surgery in prion diseases. *Emerg Infect Dis* **13**, 162-164.

[8] den Haan J, Morrema THJ, Rozemuller AJ, Bouwman FH, Hoozemans JJM (2018) Different curcumin forms selectively bind fibrillar amyloid beta in post mortem Alzheimer's disease brains: Implications for in-vivo diagnostics. *Acta Neuropathol Commun* **6**, 75.

[9] Orru CD, Soldau K, Cordano C, Llibre-Guerra J, Green AJ, Sanchez H, Groveman BR, Edland SD, Safar JG, Lin JH, Caughey B, Geschwind MD, Sigurdson CJ (2018) Prion seeds distribute throughout the eyes of sporadic Creutzfeldt-Jakob disease patients. *Mbio* **9**, e02095-18.

[10] Grimaldi A, Pediconi N, Oieni F, Pizzarelli R, Rosito M, Giubettini M, Santini T, Limatola C, Ruocco G, Ragozzino D, Di Angelantonio S (2019) Neuroinflammatory processes, A1 astrocyte activation and protein aggregation in the retina of Alzheimer's disease patients, possible biomarkers for early diagnosis. *Front Neurosci* **13**, 925.

[11] Lee S, Jiang K, McIlmoyle B, To E, Xu QA, Hirsch-Reinshagen V, Mackenzie IR, Hsiung GR, Eadie BD, Sarunic MV, Beg MF, Cui JZ, Matsubara JA (2020) Amyloid beta immunoreactivity in the retinal ganglion cell layer of the Alzheimer's eye. *Front Neurosci* **14**, 758.

[12] Veys L, Vandenabeele M, Ortuno-Lizaran I, Baekelandt V, Cuenca N, Moons L, De Groef L (2019) Retinal alpha-synuclein deposits in Parkinson's disease patients and animal models. *Acta Neuropathol* **137**, 379-395.

[13] Brigger D, Muckle RJ (1975) Comparison of Sirius red and Congo red as stains for amyloid in animal tissues. *J Histochem Cytochem* **23**, 84-88.

[14] Elghetany MT, Saleem A (1988) Methods for staining amyloid in tissues: A review. *Stain Technol* **63**, 201-212.

[15] Do JP, Cao KJ, Wei S, Laurent LC, Parast MM, Yang J (2018) Identification of patients with preeclampsia by measuring fluorescence of an amyloid-binding Aryl cyano amide in human urine samples. *Anal Chem* **90**, 14316-14320.

[16] Koronyo Y, Biggs D, Barron E, Boyer DS, Pearlman JA, Au WJ, Kile SJ, Blanco A, Fuchs DT, Ashfaq A, Frautschy S, Cole GM, Miller CA, Hinton DR, Verdooner SR, Black KL, Koronyo-Hamaoui M (2017) Retinal amyloid pathology and proof-of-concept imaging trial in Alzheimer's disease. *JCI Insight* **2**, e93621.

[17] Koronyo-Hamaoui M, Koronyo Y, Ljubimov AV, Miller CA, Ko MK, Black KL, Schwartz M, Farkas DL (2011) Identification of amyloid plaques in retinas from Alzheimer's patients and noninvasive in vivo optical imaging of retinal plaques in a mouse model. *Neuroimage* **54**(Suppl 1), S204-S217.

[18] Ngolab J, Donohue M, Belsha A, Salazar J, Cohen P, Jaiswal S, Tan V, Gessert D, Korouri S, Aggarwal NT, Alber J, Johnson K, Jicha G, van Dyck C, Lah J, Salloway S, Sperling RA, Aisen PS, Rafii MS, Rissman RA (2021) Feasibility study for detection of retinal amyloid in clinical trials: The Anti-Amyloid Treatment in Asymptomatic Alzheimer's Disease (A4) trial. *Alzheimers Dement (Amst)* **13**, e12199.

[19] Cao KJ, Kim JH, Kroeger H, Gaffney PM, Lin JH, Sigurdson CJ, Yang J (2021) ARCAM-1 facilitates fluorescence detection of amyloid-containing deposits in the retina. *Transl Vis Sci Technol* **10**, 5.

[20] Chesebro B, Trifilo M, Race R, Meade-White K, Teng C, LaCasse R, Raymond L, Favara C, Baron G, Priola S, Caughey B, Masliah E, Oldstone M (2005) Anchorless prion protein results in infectious amyloid disease without clinical scrapie. *Science* **308**, 1435-1439.

[21] Klingeborn M, Race B, Meade-White KD, Rosenke R, Striebel JF, Chesebro B (2011) Crucial role for prion protein membrane anchoring in the neuroinvasion and neural spread of prion infection. *J Virol* **85**, 1484-1494.

[22] Rangel A, Race B, Striebel J, Chesebro B (2013) Non-amyloid and amyloid prion protein deposits in prion-infected mice differ in blockage of interstitial brain fluid. *Neuropathol Appl Neurobiol* **39**, 217-230.

[23] Carare RO, Hawkes CA, Jeffrey M, Kalaria RN, Weller RO (2013) Review: Cerebral amyloid angiopathy, prion angiopathy, CADASIL and the spectrum of protein elimination failure angiopathies (PEFA) in neurodegenerative disease with a focus on therapy. *Neuropathol Appl Neurobiol* **39**, 593-611.

[24] Cao K FM, Dakanali M, Chang WM, Sigurdson CJ, Theodorakis EA, Yang J (2012) Aminonaphthlanene 2-cyanoacrylate (ANCA) probes fluorescently discriminate between amyloid-β and prion plaques in brain. *J Am Chem Soc* **134**, 17338-17341.

[25] Polymenidou M, Moos R, Scott M, Sigurdson C, Shi YZ, Yajima B, Hafner-Bratkovic I, Jerala R, Hornemann S, Wuthrich K, Bellon A, Vey M, Garen G, James MN, Kav N, Aguzzi A (2008) The POM monoclonals: A comprehensive set of antibodies to non-overlapping prion protein epitopes. *PLoS One* **3**, e3872.

[26] Schrijvers EM, Buitendijk GH, Ikram MK, Koudstaal PJ, Hofman A, Vingerling JR, Breteler MM (2012) Retinopathy and risk of dementia: The Rotterdam Study. *Neurology* **79**, 365-370.

[27] Deal JA, Sharrett AR, Rawlings AM, Gottesman RF, Bandeen-Roche K, Albert M, Knopman D, Selvin E, Wasserman BA, Klein B, Klein R (2018) Retinal signs and 20-year cognitive decline in the Atherosclerosis Risk in Communities Study. *Neurology* **90**, e1158-e1166.

[28] Baker ML, Marino Larsen EK, Kuller LH, Klein R, Klein BE, Siscovick DS, Bernick C, Manolio TA, Wong TY (2007) Retinal microvascular signs, cognitive function, and dementia in older persons: The Cardiovascular Health Study. *Stroke* **38**, 2041-2047.

[29] Liew G, Mitchell P, Wong TY, Lindley RI, Cheung N, Kaushik S, Wang JJ (2009) Retinal microvascular signs and cognitive impairment. *J Am Geriatr Soc* **57**, 1892-1896.

[30] Wong TY, Hubbard LD, Klein R, Marino EK, Kronmal R, Sharrett AR, Siscovick DS, Burke G, Tielsch JM (2002) Retinal microvascular abnormalities and blood pressure in older people: The Cardiovascular Health Study. *Br J Ophthalmol* **86**, 1007-1013.

[31] Yamada M (2000) Cerebral amyloid angiopathy: An overview. *Neuropathology* **20**, 8-22.

[32] Dagvadorj A, Petersen RB, Lee HS, Cervenakova L, Shatunov A, Budka H, Brown P, Gambetti P, Goldfarb LG (2002) Spontaneous mutations in the prion protein gene causing transmissible spongiform encephalopathy. *Ann Neurol* **52**, 355-359.

[33] Krasnianski A, Heinemann U, Ponto C, Kortt J, Kallenberg K, Varges D, Schulz-Schaeffer WJ, Kretzschmar HA, Zerr I (2016) Clinical findings and diagnosis in genetic prion diseases in Germany. *Eur J Epidemiol* **31**, 187-196.

[34] Kim MO, Takada LT, Wong K, Forner SA, Geschwind MD (2018) Genetic PrP prion diseases. *Cold Spring Harb Perspect Biol* **10**, a033134.

[35] Ortuno-Lizaran I, Beach TG, Serrano GE, Walker DG, Adler CH, Cuenca N (2018) Phosphorylated alpha-synuclein in the retina is a biomarker of Parkinson's disease pathology severity. *Mov Disord* **33**, 1315-1324.

[36] Dumitrascu OM, Lyden PD, Torbati T, Sheyn J, Sherzai A, Sherzai D, Sherman DS, Rosenberry R, Cheng S, Johnson KO, Czeszynski AD, Verdooner S, Frautschy S, Black KL, Koronyo Y, Koronyo-Hamaoui M (2020) Sectoral segmentation of retinal amyloid imaging in subjects with cognitive decline. *Alzheimers Dement (Amst)* **12**, e12109.

[37] Sigurdson CJ, Nilsson KP, Hornemann S, Manco G, Polymenidou M, Schwarz P, Leclerc M, Hammarstrom P, Wuthrich K, Aguzzi A (2007) Prion strain discrimination using luminescent conjugated polymers. *Nat Methods* **4**, 1023-1030.

[38] Cao K, Farahi M, Dakanali M, Chang WM, Sigurdson CJ, Theodorakis EA, Yang J (2012) Aminonaphthalene 2-cyanoacrylate (ANCA) probes fluorescently discriminate between amyloid-beta and prion plaques in brain. *J Am Chem Soc* **134**, 17338-17341.

[39] Cao KJ, Elbel KM, Cifelli JL, Cirera J, Sigurdson CJ, Paesani F, Theodorakis EA, Yang J (2018) Solvation-guided design of fluorescent probes for discrimination of amyloids. *Sci Rep* **8**, 6950.